Boundary-Layer Meteorology (2005) 115: 27–45

INVESTIGATION OF LOW-FREQUENCY PERTURBATIONS INDUCED BY A STEEP OBSTACLE

D. CAVA[1,*], S. SCHIPA[1] and U. GIOSTRA[2]
[1]*CNR – Institute of Science of Atmosphere and Climate, Lecce, Italy;* [2]*Environmental Science Faculty, University of Urbino, Italy*

(Received in final form 1 July 2004)

Abstract. Flow perturbation due to the orographic forcing at the top of a steep ridge has been investigated. Spectral and wavelet analyses of longitudinal and vertical wind velocity components highlight the presence of low-frequency perturbations produced by topography. Wavelet kurtosis reveals the intermittent character of these perturbations. The application of a multi-resolution data filter allows the detection of the topographically forced structures and the consequent statistical characterisation. The detected topographically forced structures remain active only for a 15% of the time on average. Nevertheless, they appear very efficient in the momentum transport, accounting for about 50% of the downward momentum flux produced in the low frequency range. Quadrant analysis highlights how topographical forcing produces the weakening of ejections and the strengthening of sweeps at the top of the ridge.

Keywords: Complex terrain, Complex turbulence, Large-scale intermittence, Orographic forcing, Quadrant analysis, Wavelet analysis.

1. Introduction

The structure of turbulence over flat and homogeneous terrain has been widely investigated; the main features are nowadays well understood through both theoretical studies (e.g., Kolmogorov, 1941, 1962) and experimental results (e.g., Kaimal et al., 1972, 1976).

Orography (or, more generally, horizontal inhomogeneities) produces flow perturbations at different spatial scales. However, small scales (i.e., scales in the inertial subrange) quickly reach a local equilibrium with the changing surface characteristics, whereas large scales (i.e., scales in the production range or larger) have a longer memory of the perturbation (Panofsky et al., 1982).

In regard to gentle obstacles, perturbations have been analysed through both theoretical models and measurements (see, Carruthers and Hunt (1990) and Wood (2000) for general reviews). Although the understanding of the problem is not complete, the main features of the topic are largely accepted. On the contrary, the understanding of the flow interaction with steep

* E-mail: d.cava@isac.cnr.it

obstacles is at a preliminary stage (Simpson, 1989; Wood and Mason, 1993; Tampieri et al., 2003). New insights could be obtained by experiments in simplified conditions and/or by using advanced data analysis techniques.

Our work is aimed at characterising the structure of perturbations induced on the flow by the interaction with a steep, but simplified, obstacle. To achieve this goal, wind velocity data collected at the top of a sharp ridge in Antarctica have been analysed. The experiment is characterised by favourable conditions: (i) the obstacle is a steep quasi-bidimensional ridge, orthogonal to the main flow; (ii) the flow is almost constant in intensity and direction for long periods (few days); (iii) the upstream flow crosses a 35 km homogeneous and flat wide region. However, the experiment is penalised by: (i) a sharp change in the roughness length; (ii) an enhanced asymmetry of the upstream and downstream sides of the obstacle; (iii) only two measurement points are available: the first, on the obstacle crest; the second, 4 km upstream of the obstacle.

Flow interaction with steep obstacles produces non-linear effects that can lead to intermittency, or even to upstream and downstream separation of the flow. These processes have been investigated by using spectral and wavelet techniques. Wavelet analysis is a well-based technique in geophysical studies, especially for application to nonstationary and intermittent signals (Kumar and Foufoula-Georgiou, 1997). For its good localisation properties, wavelet analysis has been frequently used in atmospheric turbulence applications in order to study energy cascade, small-scale intermittency and coherent structures (Collineau and Brunet, 1993; Howell and Mahrt, 1994a, b; Katul et al., 1994; Katul and Vidakovic, 1996). A further technique, based on a wavelet and quadrant analysis combination, has been proposed in order to investigate the transport properties of turbulent eddies at different scales and in order to study the transition from the anisotropy of energy containing eddies to the isotropy of the inertial subrange scales (Giostra et al., 2002).

The application of quadrant and wavelet analyses to our data highlights the presence of large-scale perturbations produced by topography. Therefore, an adaptive multi-resolution data filter (Howell and Mahrt, 1994b) has been applied to detect and to statistically characterise these low frequency structures. The subsequent analysis allowed a better understanding of the structure of the perturbation, and the contribution of the perturbation to the kinetic energy and to the momentum flux has been estimated.

2. Experimental Site and Data

Observation were made during the austral summer (from December 2 , 1998, to January 19, 1999) near the highest point of Inexpressible Island (hereinafter, Inex), a ridge located on the Nansen Ice Sheet (NIS) area in Antarctica

(Figure 1a). NIS is a nearly flat region of 35×70 km^2 surrounded by mountains rapidly rising towards the Antarctic Plateau on the west, north, and north-east, by the Northern Foothills on the east, and bordered by open sea on the south. In this homogeneous area two major glaciers converge: the Reeves glacier (from the north-west) and the Priestley glacier (from the north), which frequently convey persistent katabatic winds. NIS is characterised by an almost homogeneous snowy surface.

Inex is a sharp rocky ridge (Figure 1b) of 5×13 km^2 with an elongated shape along the north-south direction. The plot of elevation across the

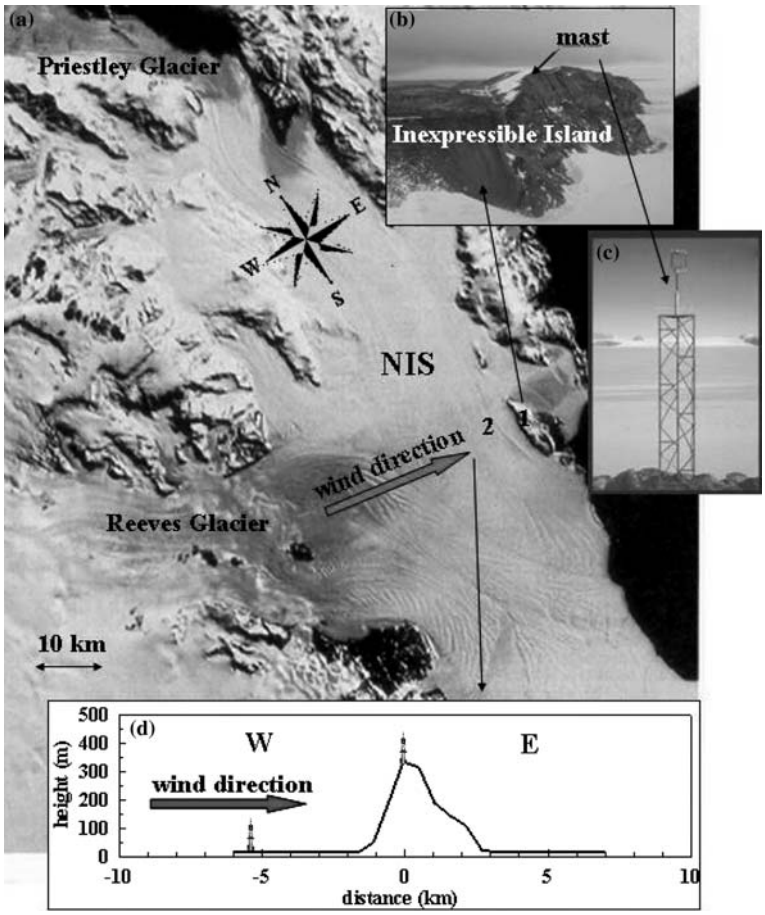

Figure 1. (a) Satellite image of the Victoria Land region in West Antarctica. Site 1 indicates the position of the mast at the top of Inex; Site 2 indicates the position of the mast located 4 km upstream of Inex; (b) picture of Inex taken from north to north-west; (c) the mast at the top of Inex taken from east toward west; the white strip visible at the horizon is the Reeves Glacier; (d) elevation plot of Inex from west to east transect; the positions of the masts (not in scale) at the top and upstream of the ridge are also indicated.

TABLE 1

Speed-up, and the ratio between the values at the crest and upstream the ridge of the friction velocity and of the longitudinal and vertical velocity component standard deviations.

DS	u_*/u_{*0}	σ_u/σ_{u0}	σ_w/σ_{w0}
0.2 ± 0.1	2.1 ± 0.2	2.2 ± 0.2	2.2 ± 0.2

west–east transect highlights the slopes and the asymmetric shape of the obstacle (Figure 1c).

Two masts were available: one was located at the top of Inex (site 1 in Figure 1a) on the western flank, where the ridge is very steep (60%) with a maximum height of 390 m (see Figure 1d); the other was located about 4 km upstream of the obstacle (site 2 in Figure 1a). The masts were equipped with symmetric three-axis ultrasonic anemometers (Gill Instruments Ltd.) at a measurement height of 2 m. The wind velocity components (u, v, w) were collected at a sampling frequency of 20.8 Hz. Data were aligned with local streamlines following McMillen (1988).

More than one hundred time series of 52 min each (2^{16} data) have been selected on the base of two criteria: (i) wind direction perpendicular to the main axis of the obstacle, i.e., winds flowing from the Reeves glacier (270° to 290°), and (ii) the atmospheric stability, with near-neutral conditions ($-0.5 < z/L < 0.5$, z being the measurement height and L the Obukhov length). Atmospheric stability has been estimated by using data collected at the upstream site. Selected periods were characterised by strong winds (more than 8 m s^{-1}). Comparison of some mean flow characteristics at sites 1 and 2 are reported in Table I; the speed-up, as well as the ratio of the other quantities, is in accordance with literature values (e.g., Kaimal and Finnigan, 1994, p. 182).

3. Velocity Spectra

Mean longitudinal and vertical velocity spectra computed by the Fast Fourier Transform (FFT) for the selected time series are shown in Figure 2. Trends and low-frequency oscillations on periods longer than 30 min were spectrally filtered out; the resolved frequency bandwidth ranges from 5×10^{-4} Hz to 10.4 Hz.

Firstly, we will briefly discuss some characteristics of the upstream flow. The spectrum of the longitudinal velocity (Figure 2a) displays a shift of the maximum towards a lower reduced frequency ($f_{max} \approx 0.008$) with respect to the theoretical value obtained from the literature in the case of the neutral boundary layer over homogeneous and flat terrain ($f_{max} \approx 0.046$). This increment of energy, also weakly observed in the vertical velocity spectrum (Figure 2b), is generated when the flow is along the Reeves glacier. These

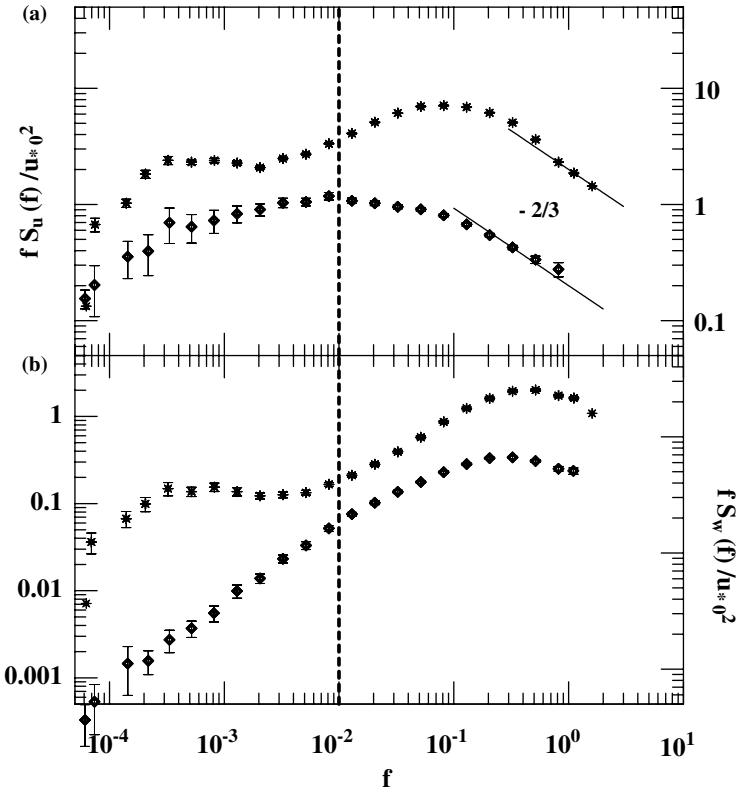

Figure 2. Longitudinal (a) and vertical (b) wind velocity spectra relative to the selected time series, normalised by the upstream u_*, versus the reduced frequency ($f = nz/U$, where n is the frequency in Hz, z is the measurement height and U is the mean longitudinal velocity). Stars represent the mean values relative to data collected at the top of Inex, whereas diamonds represent the mean values relative to data collected upstream of Inex. Vertical bars refer to the standard deviation of the mean. Continuous lines represent the $-2/3$ slope theoretically predicted in the inertial subrange (Kolmogorov, 1941). The vertical dashed lines indicate the threshold value ($f_t = 10^{-2}$) in the normalised frequency chosen for separating the *turbulent region* ($f > f_t$) from the *topographically perturbed region* ($f < f_t$) (Section 4.1).

flow characteristics were discussed previously by analysing data collected on the NIS at the Reeves glacier base (Cava et al., 2001).

Here, however, our investigation has concentrated on the perturbation induced on the incident flow (i.e., flow measured at site 2) by the steep bidimensional obstacle (i.e., Inex). Therefore, measurements collected at sites 1 and 2 have been compared. The main differences in both longitudinal and vertical velocity spectra are related to, (i) the increased kinetic energy at the obstacle crest (Table I), and (ii) the different energy distribution as a function of the reduced frequency. In particular, the peak of longitudinal spectrum shifts toward higher frequencies ($f_{max} \approx 0.08$), according to the framework of

the rapid distortion theory (Panofsky et al., 1982; Carruthers and Hunt, 1990). Above all, a marked secondary maximum is evident in the low frequency range in the spectra of both velocity components.

Secondary maxima are localised in the range 10^{-4} to 10^{-3} of reduced frequency and they are both separated from the turbulence maxima by a spectral gap.

As is well-known, flow interaction with steep obstacles can produce coherent structures and can lead to the detachment or intermittency in the flow (see, for example, Simpson, 1989). Therefore, in order to investigate the large-scale motions induced by orography and associated with the secondary spectral maxima, the analysis of the selected time series has been performed by using more suitable techniques, that is wavelet and quadrant analyses.

4. Wavelet and Quadrant Analyses

Wavelet analysis can be used to obtain insight into the structure of the investigated scales; technical details can be found in Kumar and Foufoula-Georgiou (1997).

The Haar wavelet has been chosen for its excellent localisation in physical space; the Haar basis is given by:

$$\Psi(x) = \begin{cases} +1 & 0 \le x < 0.5 \\ -1 & 0.5 \le x < 1 \\ 0 & \text{otherwise.} \end{cases} \tag{1}$$

The algorithm allowing the calculation of the Haar wavelet coefficients is (Howell and Mahrt, 1994b):

$$\Delta u_i(m,k) = \frac{1}{2^m} \sum_{j=1}^{2^{m-1}} (u_i(2^m(k-1)+j) - u_i(2^m(k-1/2)+j)), \tag{2}$$

where $m = [1\ M]$ is the scale index and $k = [1\ 2^{M-m-1}]$ is the translation (or position) index, $N = 2^M$ is the number of samples, where $M = 16$, and u_i ($i = 1, 2, 3$) are the wind velocity components. Both u_i ($i = 1, 2, 3$) and (u, v, w) are used to indicate the instantaneous wind velocity components, with primes indicating the turbulent fluctuations. The differencing properties of Haar wavelet allow us to obtain explicit relationships between wavelet coefficients and the pth order moments.

4.1. Intermittence detection

Kurtosis is a useful quantity for investigating the intermittency in a flow (Frisch, 1995, pp. 122–124). Using the differencing properties of the Haar coefficients (Δu_i), the wavelet kurtosis can be defined as (Katul et al., 1994):

$$wk(f) = \frac{\langle \Delta u_i(m,k)^4 \rangle}{\langle \Delta u_i(m,k)^2 \rangle^2}, \tag{3}$$

where $f = z/r_m \equiv nz/U$ is the reduced frequency, $r_m = 2^m dy$ is the separation distance, $dy = n_s^{-1} U$, n is the frequency in Hz, n_s is the sampling frequency, z is the measurement height, and U is the mean longitudinal velocity; finally $\langle\ \rangle$, on the right-hand side of Equation (3), indicates the linear averaging operator applied to the wavelet coefficients over all values of the position index k at the scale m. The wavelet kurtosis (hereafter, *wk*) can be used to measure the importance of the tails of the probability density function of the velocity differences, that is to study the importance of intermittent events as a function of scale r_m. In particular, the departure of *wk* from the Gaussian value ($wk = 3$) indicates an increase of intermittency.

Figure 3 shows the *wk* of the longitudinal and vertical wind components; for the sake of clarity, the same variables relative to the upstream site 2 are reported as well. As is well-known, *wk* assumes values higher than the Gaussian value in the inertial subrange, because of the small-scale intermittence (Katul et al., 1994). In the upstream case, as the scale increases, *wk* tends to the Gaussian value, showing in this way the absence of strong intermittent events. On the contrary, the topographically perturbed case at the top of the ridge (site 1) exhibits an evident peak in the low frequency range, the peak being more intense in the vertical velocity component. This behaviour suggests that the large-scale topographical perturbations have an intermittent character.

In order to investigate the statistical characteristics of these perturbations, the kurtosis deviation from the Gaussian value for localising the range of the perturbed large scales has been used. We refer to the region characterised by reduced frequencies lower than 10^{-2}, as a *topographically perturbed region*; and we refer to the region characterised by reduced frequencies higher than 10^{-2} as a *turbulent region*.

4.2. Wavelet-quadrant analysis of momentum cospectrum

The quadrant analysis allows the conditional sampling of data triggered by the occurrence of dominant structures (ejections and sweeps) or by the occurrence of secondary structures (see Figure 4 for a sketch overview).

The quadrant analysis is commonly applied to the fluctuations of the wind velocity components. Nevertheless, interesting information about the relative importance of even and odd quadrants at the different scales can be obtained by applying the quadrant analysis to the wavelet coefficients of the wind velocity components at each resolved scale (Hayashi, 1994; Giostra et al.,

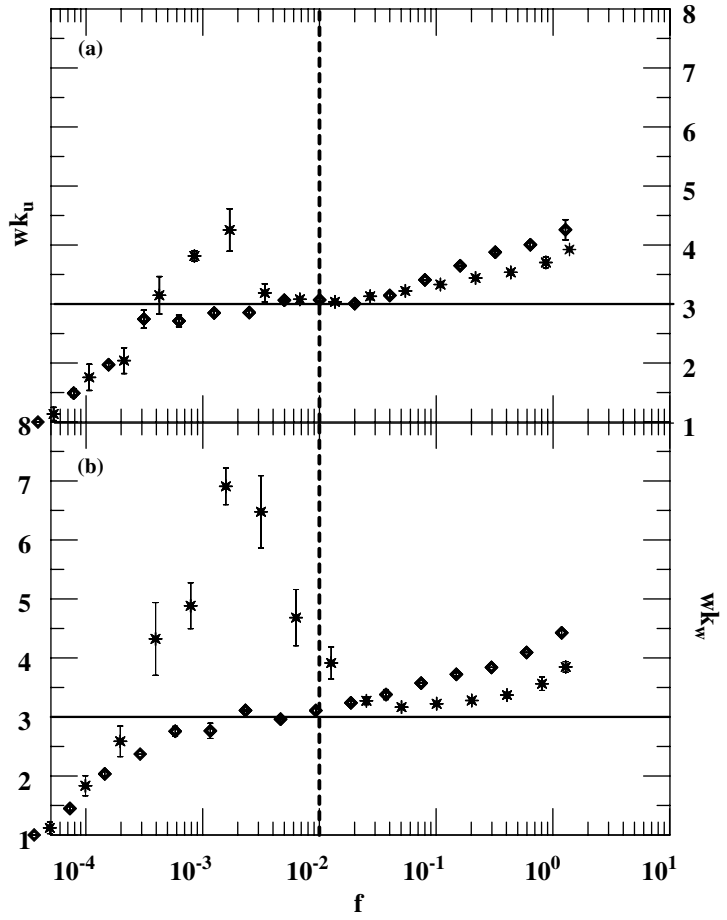

Figure 3. Wavelet kurtosis of longitudinal (a) and vertical (b) wind velocity components, versus reduced frequency. Stars represent the mean values relative to data collected at the top of Inex, whereas diamonds represent the mean values relative to data collected upstream of Inex. Vertical bars refer to the standard deviation of the mean. The vertical dashed lines indicate the threshold value ($f_t = 10^{-2}$) in the normalised frequency chosen for separating the *turbulent region* ($f > f_t$) from the *topographically perturbed region* ($f < f_t$) (Section 4.1).

2002). This technique allows the estimation of the contribution to the co-spectrum from ejections and sweeps (even quadrants) and from reflections and deflections (odd quadrants) at different spatial scales.

In a way analogous to the total wavelet momentum cospectrum, defined as:

$$C_{uw}(f) = \frac{\langle \Delta u(m,k)\Delta w(m,k)\rangle dy}{2\pi ln(2)}, \tag{4}$$

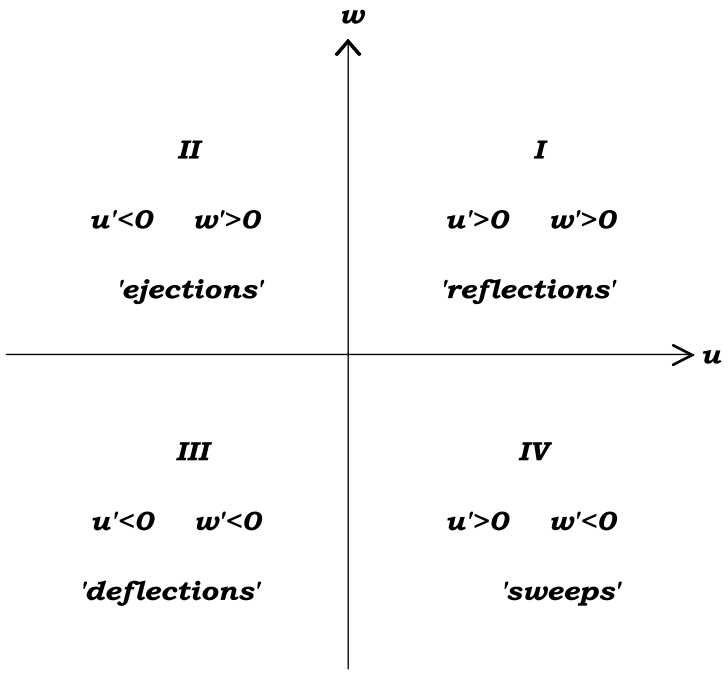

Figure 4. Ejections (quadrant II) corresponding with low speed portions of the air moving from the surface. Sweeps (quadrant IV) reflect the motion of high speed air towards the surface. Both these structures (associated to the even quadrants) give a negative momentum flux; therefore they are the dominant structures in a surface layer flow. The interaction between ejections and sweeps produces secondary flow structures (associated to the odd quadrants) that provide a positive contribution to the momentum transport. Such an interaction can occur with reflections of accelerated sweeps outwards from the surface (quadrant I) and with deflections of decelerated air portions back towards the surface (quadrant III) (Lykossov and Wamser, 1995).

the quadrant cospectrum can be defined as (Giostra et al., 2002):

$$C_{uw}{}^{(q)}(f) = \frac{\langle(\Delta u(m,k)\ \Delta w(m,k))I_{q,h}{}^{(m)}\rangle dy}{2\pi ln(2)} \tag{5}$$

using an *indicator function* ($I_{q,k}$) that sorts the contribution from each quadrant:

$$I_{q,k}{}^{(m)} = \begin{cases} 1 & \text{when } (\Delta u(m,k), \Delta w(m,k)) \text{ is in the } q \text{ quadrant} \\ 0 & \text{otherwise.} \end{cases} \tag{6}$$

The total wavelet cospectrum at the upstream site (Figure 5a) is the result of the antagonist effect of even quadrants (i.e., quadrants providing a negative contribution to the momentum flux) and odd quadrants (i.e., quadrants providing a positive contribution to the momentum flux). Even quadrants are dominant in the *turbulent region*, determining a net negative total momentum

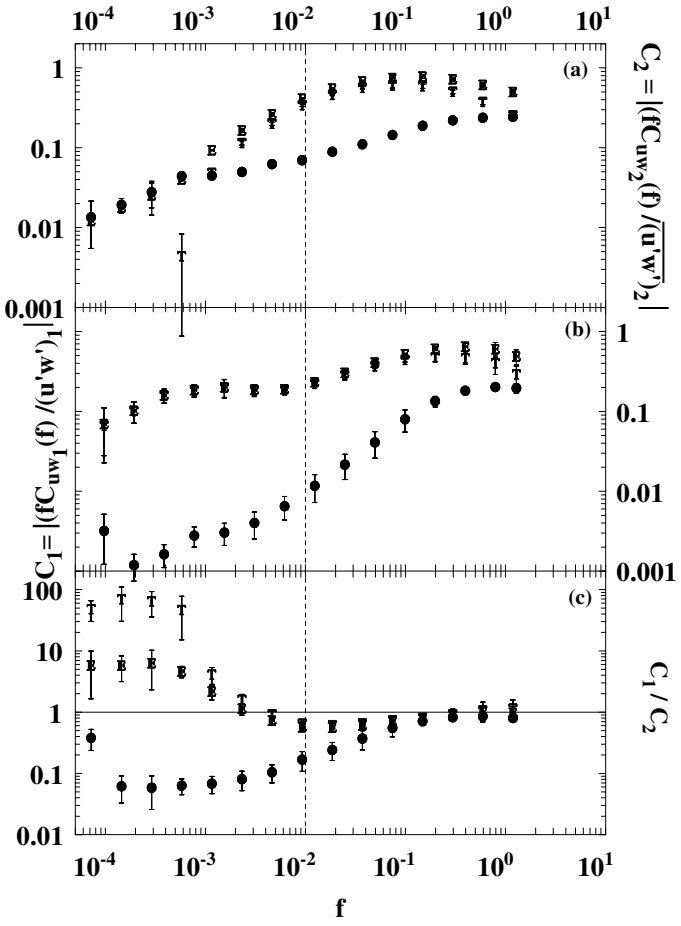

Figure 5. Vertical momentum flux cospectrum computed by the combination of wavelet and quadrant analyses, relative to the data collected at the upstream site, C_2, (a), and at the top of Inex, C_1, (b); the ratio between the two normalised C_1/C_2 is also shown (c). (T) indicates the total momentum flux; (O) and (E) indicate the odd and even quadrants contributions, respectively. Symbols represent the mean values relative to the selected time series. Vertical bars refer to the standard deviation of the mean. The vertical dashed lines indicate the threshold value ($f_t = 10^{-2}$) in the normalised frequency chosen for separating the *turbulent region* ($f > f_t$) from the *topographically perturbed region* ($f < f_t$) (Section 4.1).

flux in that region. At lower frequencies, even and odd quadrants have the same magnitude, leading to an almost zero total momentum cospectrum.

The wavelet and quadrant analyses of the momentum cospectrum at the crest of the ridge (Figure 5b) highlight a behaviour analogous to the upstream case in the *turbulent region*. On the contrary, in the *topographically perturbed region* the total cospectrum exhibits a secondary maximum and it is completely driven by the even quadrants; that is, the (downward) momentum

transport in this region is completely driven by motions organised in ejection and sweep cycles. In fact, the cospectrum associated with odd quadrants quickly collapses to zero as the reduced frequency increases.

Finally, Figure 5c shows the ratio between the normalised cospectra computed at the ridge top and the normalised cospectra computed upstream of the obstacle. This ratio is about equal to one in the *turbulent region*, indicating a behaviour of the normalised cospectra that is quite similar. On the contrary, the increase of the ratio in the *topographically perturbed region* highlights the large-scale stress perturbation induced by the interaction of the flow with the obstacle.

5. Detection of Topographically Forced Structures

The performed analysis has shown that flow interaction with the steep obstacle produces perturbations in the low frequency range. These perturbations have an intermittent character and contribute to the kinetic energy and to the momentum flux. Moreover they are organised in ejection-sweep cycles, and hereafter we refer to them as topographically forced structures (*tfs*).

In order to statistically characterise the intermittent *tfs*, the adaptive multi-resolution data filter proposed by Howell and Mahrt (1994a) has been applied to the data. The filter acts as a running mean that removes small-amplitude and small-scale variations in the signal, but retains changes associated to large-scale structures. The fine-structure turbulence plays a leading role both in the energetic contribution and in the momentum transport. Therefore, in order to extract *tfs*, the application of a lowpass filter to the signal before using the adaptive multi-resolution data filter has been needed. According to the previous analysis (refer Section 4.1), a threshold $f_t = 10^{-2}$ in the reduced frequency has been chosen to filter out the turbulence contribution. As stated before (Section 4.2), the *tfs* appear associated with a strong increase of the momentum flux. Consequently, in order to better isolate the *tfs*, the largest magnitudes of the product of longitudinal and vertical wavelet coefficients ($\Delta u(m, k)\Delta w(m, k)$) have been detected by applying the adaptive multi-resolution data filter (see Howell and Mahrt, 1994a, b, for technical details relative to the detection procedure). As a result, the signal corresponding with frequencies lower than the threshold value can be decomposed (Figure 6) into a component associated with the *tfs* and into a component associated with the residual; for convenience, we refer to the latter component as the *unperturbed large scales*. In particular, the $u'w'$ plot highlights the intense, even if sporadic, contribution due to the *tfs*, as well as the weak, even if persistent, contribution due to the *unperturbed large scales*.

It is noteworthy that *no tfs* has been detected by applying the same procedure to the low frequency range of data collected at the upstream site (site 2).

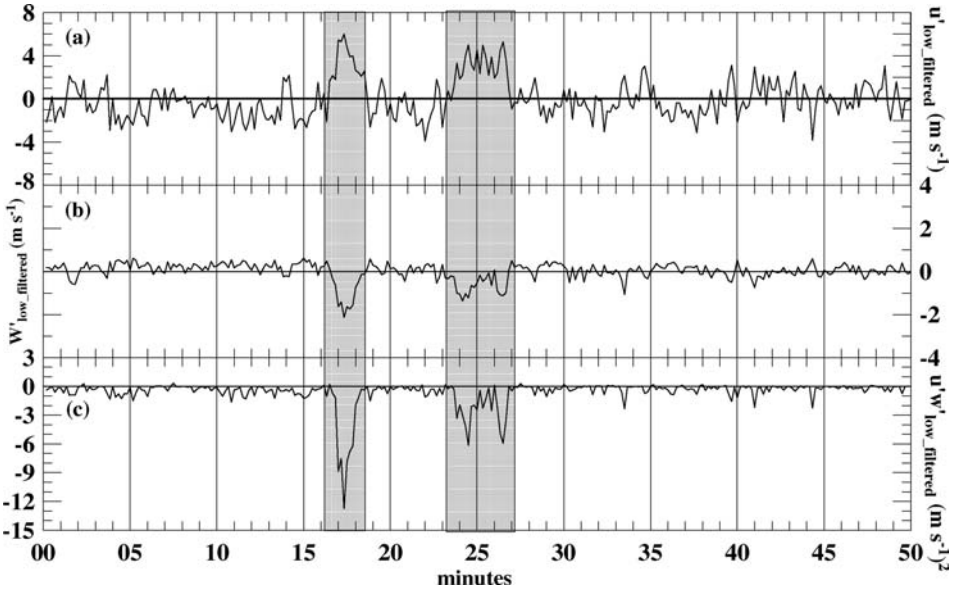

Figure 6. Instantaneous signals corresponding with frequencies lower than the threshold value ($f_t = 10^{-2}$) for longitudinal wind velocity component (a), vertical wind velocity component (b), and momentum flux (c), relative to a 52-min run collected on December 23, 2200 to 2250 (local time). Shaded areas refer to the *tfs* detected applying the multi-resolution data filter.

6. Statistical characterisation of topographically forced structures

The procedure described in the previous section has been applied to the complete dataset of site 1 in order to statistically characterise the detected *tfs*. The distribution of the time interval between *tfs* (Figure 7) is characterised by a mode of 4 min and an average of about 11 min. The tail of distribution highlights the presence of quiescent periods between two consecutive structures longer than half an hour.

Applying the frozen turbulence hypothesis, the distribution of the horizontal dimension of the detected events (Figure 8) is characterised by a dominant scale of about 800–1,000 metres.

This length scale is of the same order as horizontal scale of the obstacle upstream side (see, Figure 1d). We can define an intermittency index as the ratio of the duration of the structure (i.e., the fraction of the record occupied by the structure component) to the total record length (Hagelberg and Gamage, 1994). On the basis of this definition, the topographical structures remain active on average for a 15% of the time (Figure 9).

Figure 10 shows the distribution of the percentage of longitudinal variance relative to the *fine structure turbulence* (a), to the *tfs* (b) and to the *unperturbed large scales* (c). In an analogous way, Figures 11 and 12 refer, respectively, to

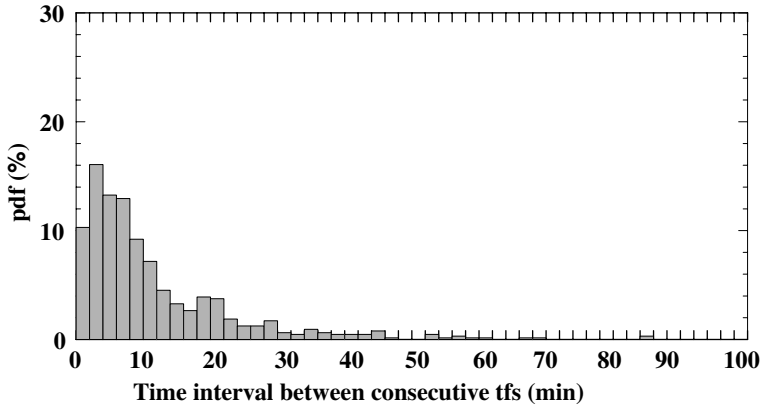

Figure 7. Distribution of time interval between consecutive *tfs* detected by multi-resolution data filter.

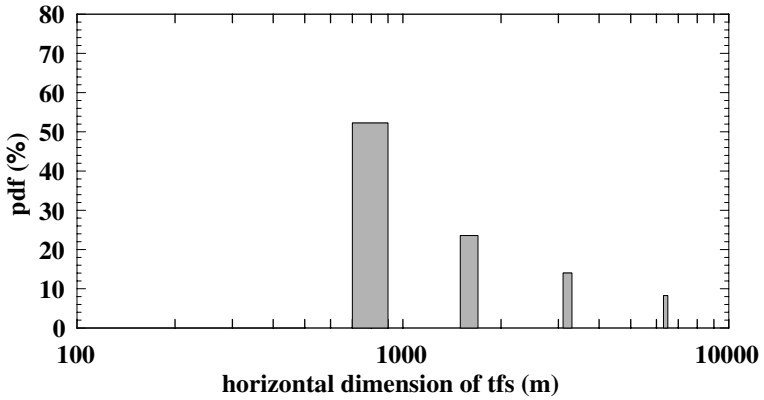

Figure 8. Distribution of horizontal dimension of *tfs* detected by multi-resolution data filter.

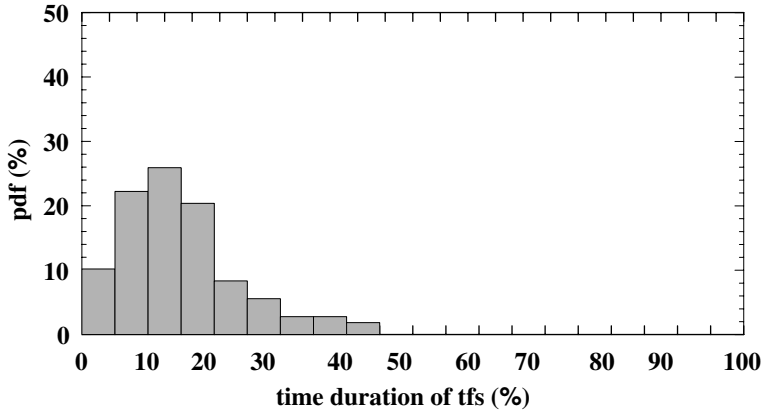

Figure 9. Distribution of the time duration of the *tfs* detected by multi-resolution data filter.

the distribution of the percentage of the vertical velocity variance and of the momentum flux. As expected, the *fine structure turbulence* accounts for the greatest contribution to the energy and to the momentum flux. Although *tfs*

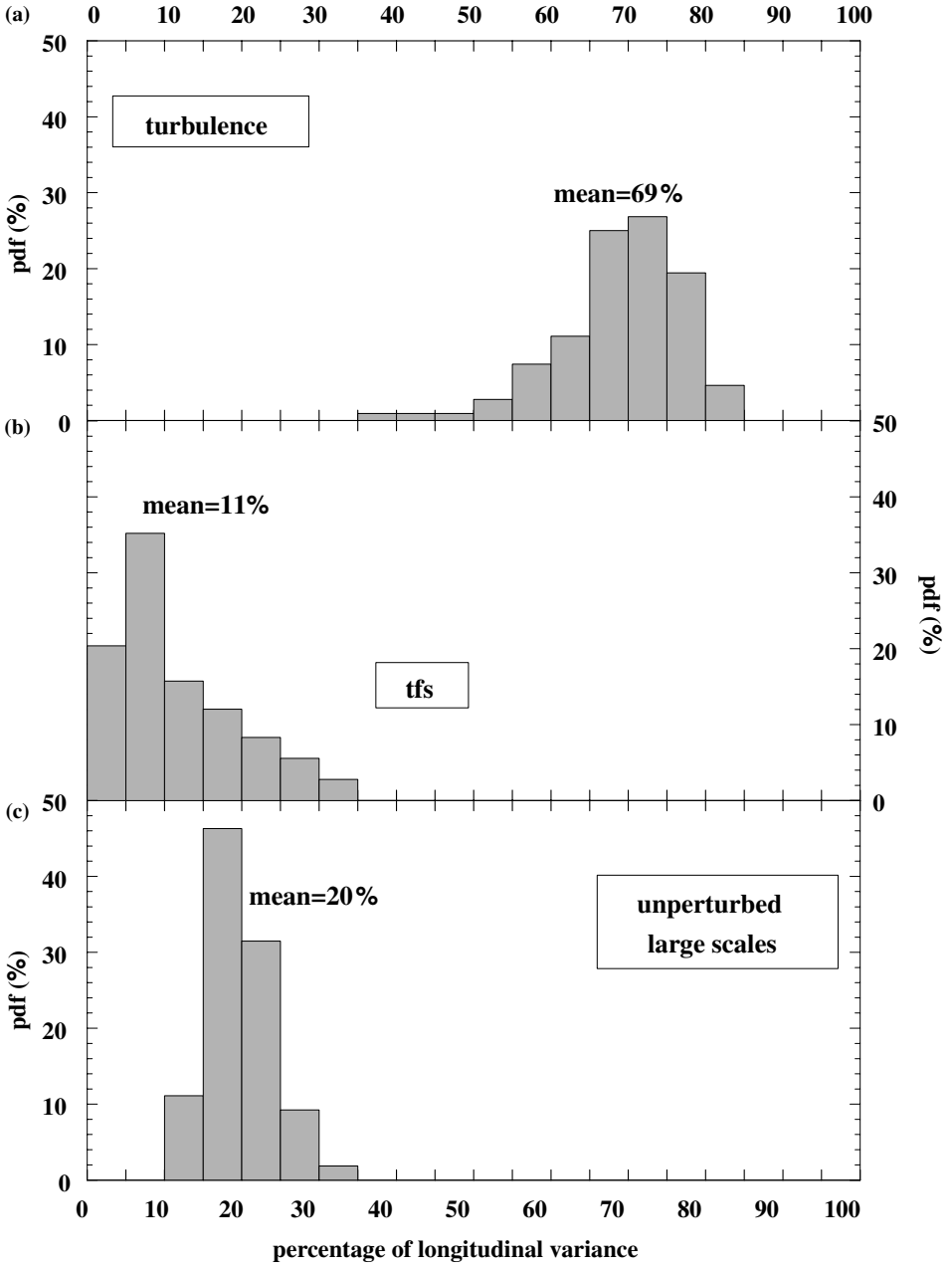

Figure 10. Distribution of the percentage of longitudinal variance relative to the fine-structure turbulence (a), to the *tfs* (b) and to the unperturbed large scales (c).

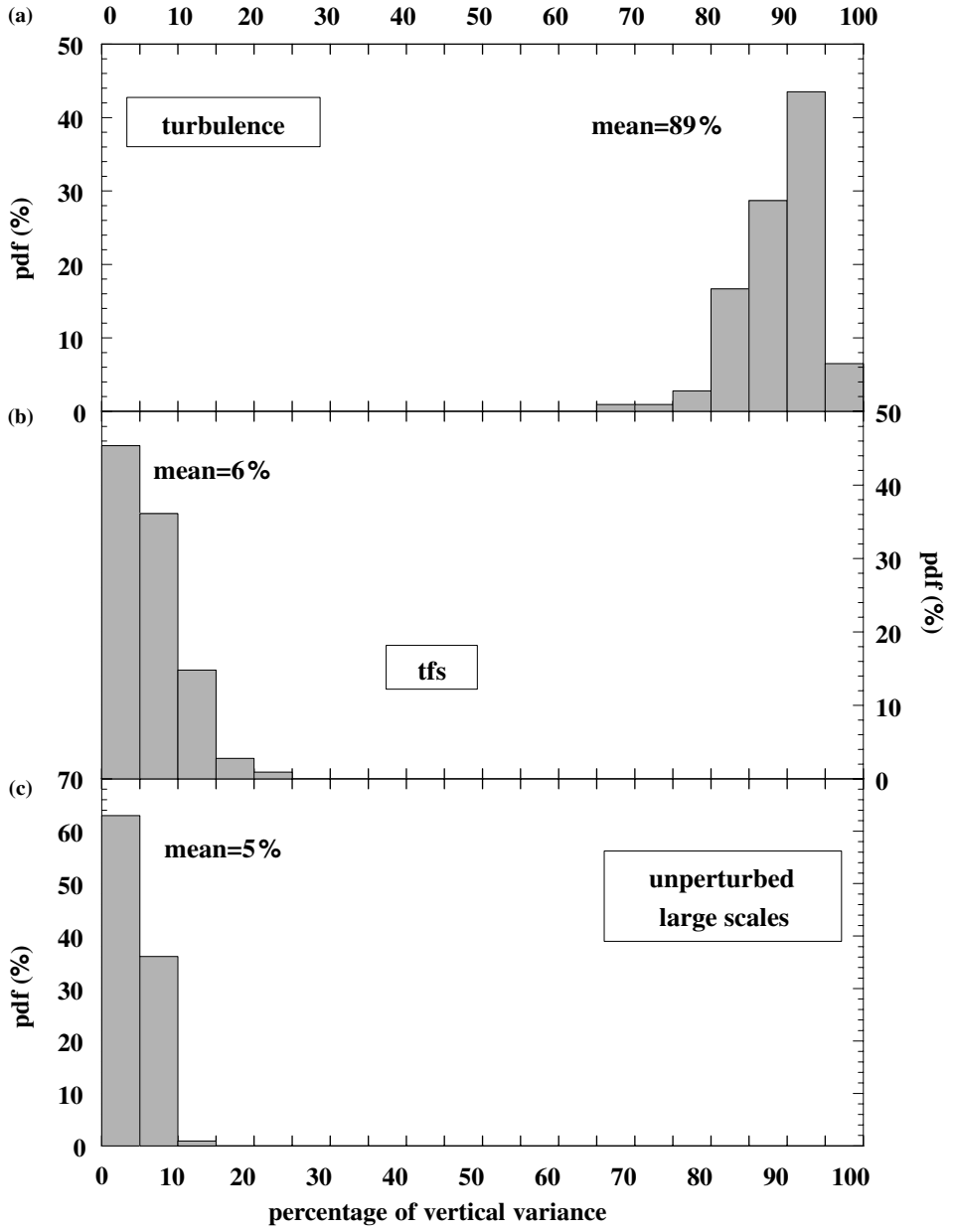

Figure 11. As Figure 10, but for vertical velocity variance.

remain active for only 15% of the time, their contribution to the flow energy and to the momentum flux is comparable to that of the more persistent *unperturbed large scales*. As a matter of fact, *tfs* account for about 50% of the

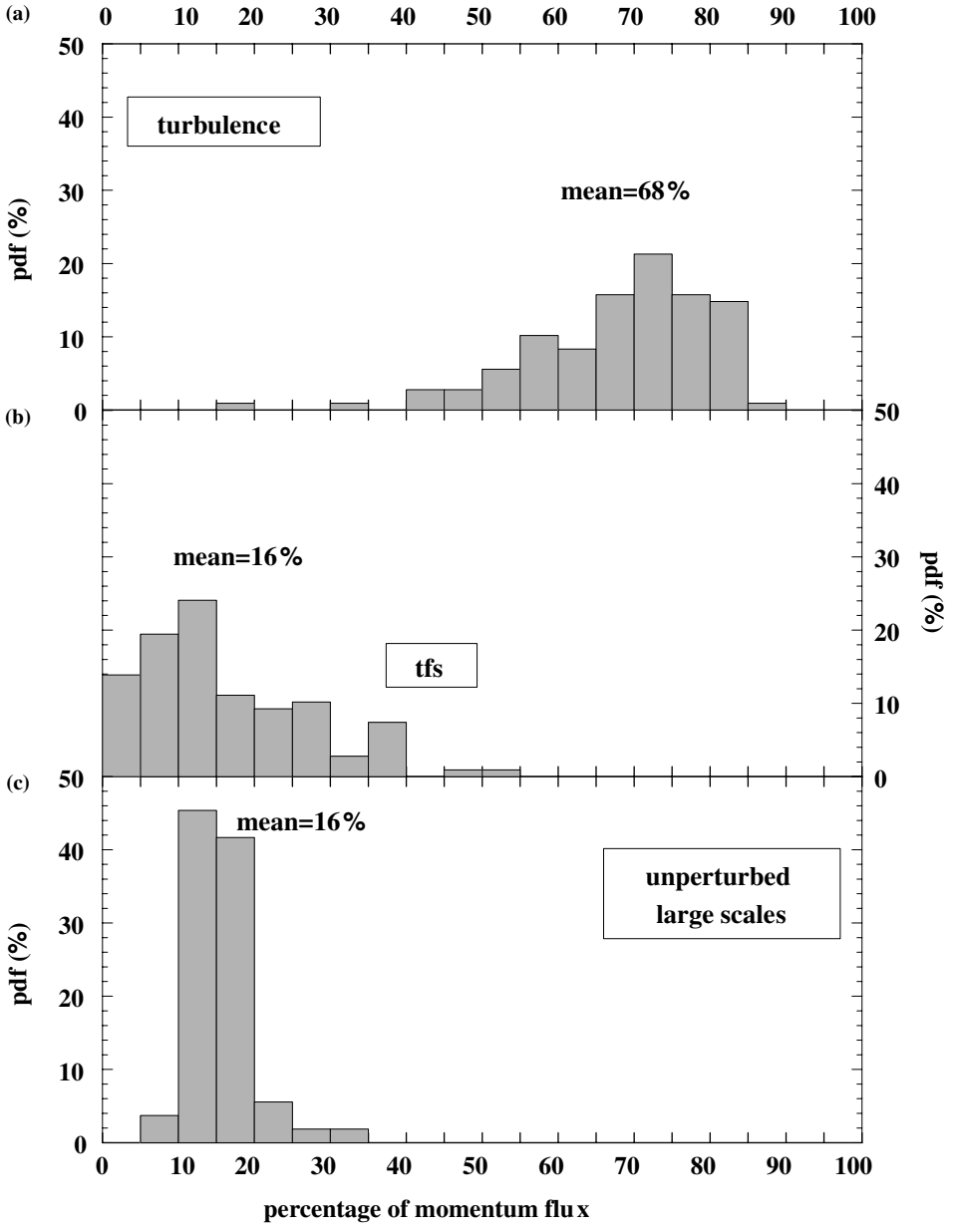

Figure 12. As Figure 10, but for momentum flux.

downward momentum flux produced in the low frequency range corresponding to about 16% of the total value.

Finally, the distribution of the occurrence frequency relative to the four quadrants for detected events is shown in Figure 13. About 70% of the

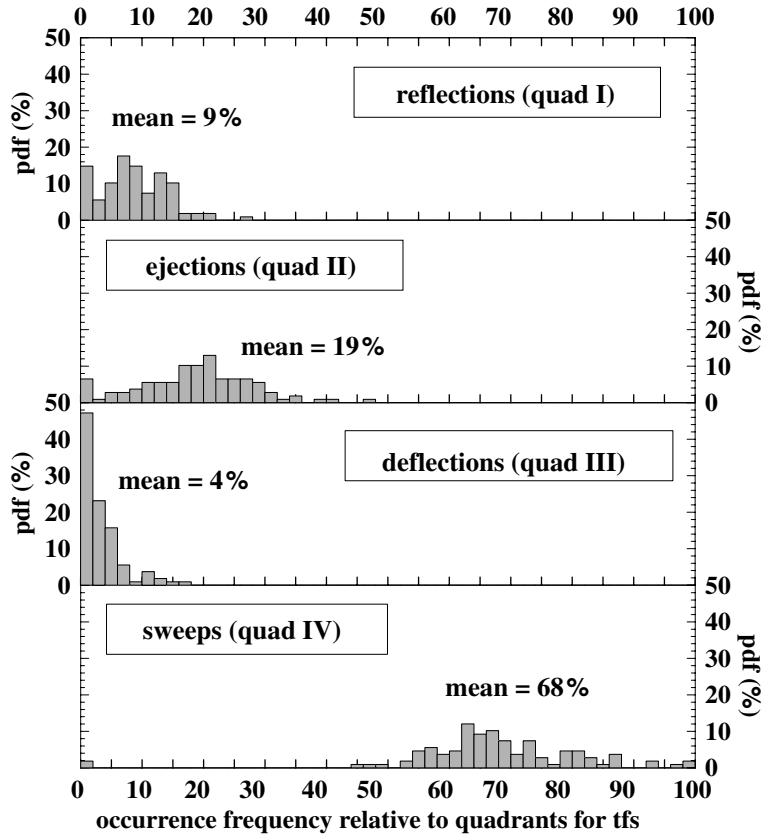

Figure 13. Distribution of the occurrence frequency relative to the four quadrants for *tfs* detected by multi-resolution data filter.

topographically forced structures are associated with sweeps, whereas only 20% are associated with ejections. As expected, odd quadrants are active only for a small fraction of time.

7. Conclusions

Wind velocity data collected at the top of a sharp ridge show an increase in spectral energy in the low frequency subrange. The aim of our study has been to investigate and to characterise perturbations induced by flow-topography interaction.

A wavelet analysis and a multi-resolution data filter have been respectively applied in order to select the spectral range perturbed by the orography and in order to detect the intermittent structures induced by the orography itself. The wavelet analysis applied to the kurtosis of the longitudinal and vertical

wind components, clearly identifies the low frequency spectral range affected by the occurrence of intermittent topographically forced structures (*tfs*).

The wavelet-quadrant analysis applied to the momentum cospectrum highlights how these intermittent *tfs* are related to ejection-sweep cycles; therefore, their main contribution is a strong and negative momentum transfer in the low frequency spectral subrange.

The detection of *tfs*, by the application of the multi-resolution data filter, allows a better comprehension of their statistical characteristics, in terms of their intermittent occurrence, of their mean duration, and of their efficiency in transporting momentum flux. The performed analysis shows that *tfs* are characterised by a mean duration of about 1–2 min and a typical horizontal dimension of about 800 m. This horizontal dimension is of the same order as the horizontal scale of the upstream side of the obstacle.

Tfs remain active only for 15% of the total time, but, nevertheless, are very efficient in the momentum transport, contributing to 50% of the low frequency momentum flux. Finally, quadrant analysis revealed that the intermittent *tfs* are mainly associated with sweeps and that they produce a weakening of ejections at the top of the ridge.

Because sweeps are associated with accelerated downward motions, their dominant behaviour could be due to a tilting of the instantaneous streamlines (with respect to the mean streamline), as a consequence of the intermittent occurrence of an upwind separation region.

Further and more complete experimental investigations are needed to understand the structure of perturbations induced by flow interaction with a steep obstacle. Nevertheless, the proposed analysis technique appears to be a powerful tool for approaching this complex topic.

Acknowledgements

Authors are grateful to A. Maurizi, M. Tagliazucca and F. Tampieri, for fruitful discussions. The suggestions of the anonymous referees are also gratefully acknowledged. This work was carried out in the frame of the Italian National Program for Research in Antarctica (PNRA), and was partially supported by the Italian National Research Council (CNR) in the frame of Arctic Project.

References

Carruthers, D. J. and Hunt, J. C. R.: 1990, 'Fluid Mechanics of Airflow over Hills: Turbulence, Fluxes, and Waves in the Boundary Layer', in W. Blumen (ed.), *Atmospheric Processes over Complex Terrain*, AMS, Boston, pp. 83–103.

Cava, D., Giostra, U., and Tagliazucca, M.: 2001, 'Spectral Maxima in a Perturbed Atmospheric Boundary Layer', *Boundary-Layer Meteorol.* **100**, 421–437.

Collineau, S. and Brunet, Y.: 1993, 'Detection of Turbulent Coherent Motions in a Forest Canopy, I, Wavelet Analysis', *Boundary-Layer Meteorol.* **65**, 357–379.

Frisch, U.: 1995, *Turbulence, The Legacy of A. N. Kolmogorov*, Cambridge University Press, Cambridge, 296 pp.

Giostra, U., Cava, D., and Schipa, S.: 2002, 'Structure Functions in a Wall-Turbulent Shear Flow', *Boundary-Layer Meteorol.* **103**, 337–359.

Hagelberg, C. R. and Gamage N. K. K.: 1994, 'Structure-Preserving Wavelet Decompositions of Intermittent Turbulence', *Boundary-Layer Meteorol.* **70**, 217–246.

Hayashi, T.: 1994, 'An Analysis of Wind Velocity Fluctuations in the Atmospheric Surface Layer Using an Orthonormal Wavelet Transform', *Boundary-Layer Meteorol.* **70**, 307–326.

Howell, J. F. and Mahrt, L.: 1994a, 'An Adaptive Multiresolution Data Filter: Applications to Turbulence and Climatic Time Series', *J. Atmos. Sci.* **51**, 2165–2178.

Howell, J. F. and Mahrt, L.: 1994b, 'An Adaptive Decomposition: Application to Turbulence', in E. Foufoula-Georgiou and P. Kumar (eds.), *Wavelets in Geophysics*, Academic Press, San Diego, CA, pp. 107–128.

Kaimal, J. C. and Finnigan, J. J.: 1994, *Atmospheric Boundary Layer Flows: Their Structure and Measurement*, Oxford University Press, Oxford, 289 pp.

Kaimal, J. C., Wyngaard, J. C., Haugen, D. A., Coté, O. R., Izumi, Y., Caughey, S. J., and Readings, C. J.: 1976, 'Turbulence Structure in the Convective Boundary Layer', *J. Atmos. Sci.* **33**, 2152–2169.

Kaimal, J. C., Wyngaard, J. C., Izumi, Y., and Coté, O. R.: 1972, 'Spectral Characteristics of Surface Layer Turbulence', *Quart. J. Roy. Meteorol. Soc.* **98**, 563–589.

Katul, G. G. and Vidakovic, B.: 1996, 'The Partitioning of Attached and Detached Eddy Motion in the Atmospheric Surface Layer Using Lorentz Wavelet Filtering', *Boundary-Layer Meteorol.* **77**, 153–172.

Katul, G. G., Albertson, J. D., Chu, C. R., and Parlange, M. B.: 1994, 'Intermittency in Atmospheric Turbulence Using Orthonormal Wavelets', in E. Foufoula-Georgiou and P. Kumar (eds.), *Wavelets in Geophysics*, Academic, San Diego, CA, pp. 81–105.

Kolmogorov, A. N.: 1941, 'The Local Structure of Turbulence in Incompressible Viscous Fluid for Very Large Reynolds Number', *Dokl. Akad. Nauk. SSSR,* **30**, 9–13.

Kolmogorov, A. N.: 1962, 'A Refinement of Previous Hypotheses Concerning the Local Structure of Turbulence in a Viscous Incompressible Fluid at High Reynolds Number', *J. Fluid Mech.* **13**, 82–85.

Kumar, P. and Foufoula-Georgiou, E.: 1997, 'Wavelet Analysis for Geophysical Applications', *Rev. Geophys.* **35**, 385–412.

Lykossov, V. N. and Wamser, C.: 1995, 'Turbulence Intermittency in the Atmospheric Surface Layer over Snow-Covered Sites', *Boundary-Layer Meteorol.* **72**, 393–409.

McMillen, R. T.: 1988, 'An Eddy Correlation Technique with Extended Applicability to Non-Simple Terrain', *Boundary-Layer Meteorol.* **43**, 231–245.

Panofsky, H. A., Larko, D., Lipschutz, R., Stona, G., Bradley, E. F., Bowen, A. J., and Højstrup, J.: 1982, 'Spectra of Velocity Components over Complex Terrain', *Quart. J. Roy. Meteorol. Soc.* **108**, 215–230.

Simpson, R. L.: 1989, 'Turbulent Boundary-Layer Separation', *Annu. Rev. Fluid Mech.* **21**, 205–234.

Tampieri, F., Mammarella, I., and Maurizi, A.: 2003, 'Turbulence in Complex Terrain', *Boundary-Layer Meteorol.* **109**, 85–97.

Wood, N.: 2000, 'Wind Flow over Complex Terrain: a Historical Perspective and the Prospect for Large-Eddy Modelling', *Boundary-Layer Meteorol.* **96**, 11–32.

Wood, N. and Mason, P.: 1993, 'The Pressure Force Induced by Neutral, Turbulent Flow over Hills', *Quart. J. Roy. Meteorol. Soc.* **119**, 1233–1267.